In: Proceedings of the 2016 Annual Meeting of the Adhesion Society, San Antonio, TX 2016

Cellulose Nanocrystal Reinforced Epoxy Coatings

L. Cross*, J. Marshall*, G. Schueneman** and E. Mintz*

**Department of Chemistry, Clark Atlanta University, 223 James P. Brawley Dr. S.W., Atlanta, GA 30314, lionel.cross0@gmail.com,* jamila.s.marshall@gmail.com, *emintz@cau.edu*
***Forest Service, Forest Products Laboratory, 1 Gifford Pinchot Dr., Madison, WI 53705, gtschueneman@fs.fed.us,*

Introduction

There is growing market interest in and availability of bioderived polymers and resins for use in plastics, adhesives, coatings, etc. Thus, there is an opportunity for bioderived nanomaterials to allow the production of 100% biobased polymer matrix composites (PMCs). All trees and plants utilize a nanoscale cellulose fiber as a building block in their reinforcing phase. The presence of nanofibers in cell walls was postulated in the 1920's and proven in the 1950's, being referred to at that time as an elementary fibril [1-6]. Research into the benefits of nanotechnology has resulted in worldwide attention on cellulose based nanomaterials. Results to date have shown that crystalline cellulose nanofibers, termed cellulose nanocrystals (CNCs), have modulus and tensile properties on par with aramid fiber [7]. Herein, we report the effects of incorporating CNCs from trees into a model waterborne (WB) epoxy coating.

Experimental

Materials: CNCs were provided by the US Forest Service Forest Products Laboratory (FPL) as freeze dried powder and as a 8.75 wt.% dispersion in water. The CNCs were extracted from mixed southern yellow pine dissolving pulp [8]. Typical sizes of CNCs derived from this process are 5 nm in cross section and 150±50 nm long. The CNCs in the dispersion had 0.72 wt% sulfur and the freeze dried powder had 1 wt.% sulfur as determined by inductively coupled plasma optical emission spectroscopy (ICP-OES). The epoxy (Ancarez AR555, EEW=550), aliphatic polyamine (Anquamine 401, AHEW=200), and defoamer (Surfynol DF-75 and DF-110D) were provided by Air Products (Allentown, PA).

Nanocomposite Preparation: Amine and epoxy were mixed at a 0.42 molar ratio. Aqueous CNC dispersion, defoamer, and distilled water were added directly to this mixture. The composites were cured for one day at 25°C and 2.5 hours at 120°C. CNCs were loaded into the epoxy such that the cured films had 5 and 11.6 wt.% CNCs, where 11.6 % corresponds to complete replacement of the added water in the formulation with the CNC aqueous dispersion.

Thermal Analysis: Samples were placed on the platinum pan of a TA Instruments Q50 thermogravimetric analyzer (TGA) and heated at 2, 5, 10, 15, and 20°C/min under nitrogen. Kinetic parameters were calculated using Microsoft Excel and TA Specialty Library software.

Thermal – Mechanical Analysis: A TA AR-G2 Rheometer was used to measure the modulus of the nanocomposites from 25-150°C with a 1°C/min ramp rate, and 1% oscillatory strain operating at 1 Hz using a rectangular geometry fixture.

Abrasion Resistance: Steel plates were coated with the nanocomposites and unreinforced epoxy then cured as described above. The plates were mounted on a 5190 Taber Abrader and tested in accordance with ASTM D4060-07 using CS-17 wheels with 500g weights [9]. Each of three specimens per coating type were abraded for 1000 cycles, weighed, and the wheels cleaned via 150 grit sand paper prior to starting the next 1000 cycle period for a total of 5000 cycles.

Results and Discussion

The pessimistic expectation is that thermal stability will be sacrificed when a bioderived fiber is added to an epoxy resin. This was investigated via TGA. The thermograms for the fully cured CNC composites and neat epoxy are shown Figure 1. They exhibit similar mass loss behavior until 150°C where the CNC composites begin a higher loss rate that continues up to the epoxy's decomposition onset temperature. As the temperature was scanned beyond this point the CNC composites rejoin the wt. loss profile of the epoxy at 70% wt., 350°C for the 5 wt.% composite and 63% wt., 370°C for the 11.6 wt.% composite. The difference between these points is similar to the variation in wt% loadings of the CNC composites. Thermal stability beyond these points are similar to the neat epoxy with similar and less char for the 5 and 11.6 wt.% composites, respectively. The initial increase in wt. loss results in a slight increase in wt. loss over the neat epoxy. Overall, this comparison in thermal stability reveals a favorable match for use of CNCs in WB epoxy coatings.

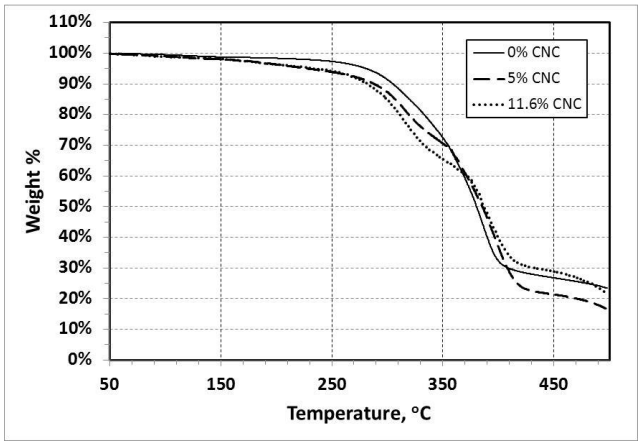

Figure 1: TGA thermoscans of epoxy and epoxy with 5 and 11.6 wt.% CNCs [10].

The practical applicability of the TGA comparison is limited as most applications require thermal stability upon exposure to prolonged isothermal conditions and often with the addition of a load. Thus, to better gauge the stability of the CNCs the kinetic parameters associated with thermal degradation of the CNCs and their starting materials were ascertained via Kissinger model-free methodology [11, 12]. This model uses the equation shown below, where β is the heating rate, T is the temperature in Kelvin, T_m is the Kelvin temperature value at the maximum of the DTG vs. temperature curve and R is the ideal gas constant.

$$\frac{d\left[ln\left(\frac{\beta}{T_m^2}\right)\right]}{d\left(\frac{1}{T_m}\right)} = -\frac{E_a}{R}$$

A graph of $\ln(\beta/T_m^2)$ versus $1/T_m$ will yield a straight line plot for the first derivative (DTG) of the individual thermogravimetric analysis curves if the model successfully fit this system. The activation energy, E_a, and pre-exponential factor, A, are obtained from the slope ($-E_a/R$) and intercept ($\ln((A*R)/E_a)$) of the equation fit to this line.

TGA experiments were carried out with varying temperature ramp rates and the material response recorded and analyzed. The DTG of the individual thermogravimetric analysis curves were recorded at 2, 5, 10, 15, 20°C/min temperature ramps. These curves give 5 maxima, one for each ramp rate, which vary as a function of temperature as shown in Figure 2. The maxima of these curves were then used to plot a graph of $\ln(\beta/T_m^2)$ versus $1/T_m$ as seen in Figure 3. This figure shows that representative experimental data fits the Kissinger model as described above. The respective half-lives were calculated using the relation $t_{½} = \ln(2)/k$. The constant k in this case is calculated using the Arrhenius equation $k = Ae^{-Ea/RT}$.

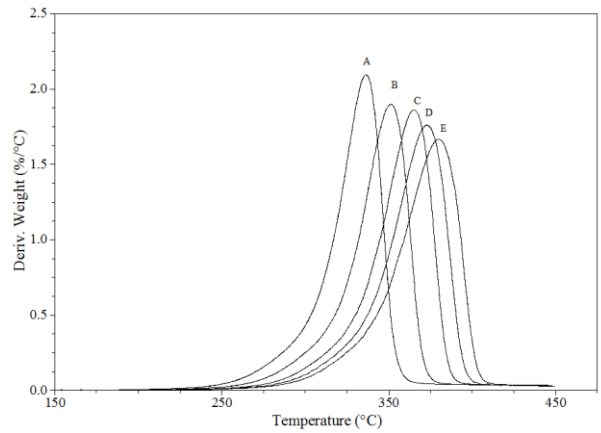

Figure 2: Representative DTG curves for the dissolving pulp used to prepare CNCs by sulfuric acid hydrolysis. Curves A, B, C, D and E represent the ramp rates of 2, 5, 10, 15, and 20 °C/min, respectively, under N_2.

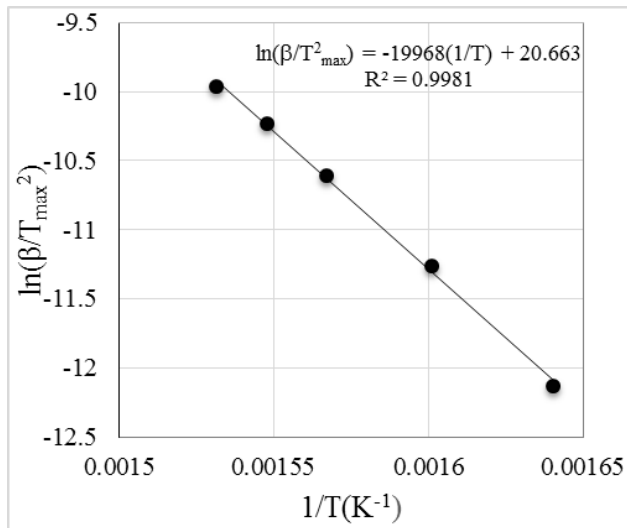

Figure 3: .Graph showing the application of the Kissinger model-free method to the dissolving pulp used to prepare CNCs by sulfuric acid hydrolysis.

Table 1. Kinetic Parameters calculated for CNCs, CNF, and the corresponding starting materials using the Kissinger Method.

Sample Name	T_d†	E_a (kJ/mol)	A (s^{-1})	$t_{1/2}$ at 165 °C ◘
Dissolving Pulp	338	166	3.13×10^{11}	2.32×10^6 min
CNCs	287	175	7.53×10^{13}	9.82×10^4 min

†: Onset of degradation (°C) at a ramp rate of 10 °C/min
◘: $t_{1/2}$ in nitrogen atmosphere

Table 1 summarizes the kinetic parameters for the source pulp that underwent sulfuric acid hydrolysis to yield the CNCs and the corresponding CNCs. The onset of degradation of the pulp is 40°C higher than the CNCs used

in this study. This contrasts with the lower activation energy of thermal decomposition found for the pulp that is offset by having a pre-exponential factor that is approximately 2 orders of magnitude lower than the CNCs. The overall impact of these properties is exhibited in the calculated half-lives ($t_{½}$) for these materials at 165°C in a nitrogen atmosphere. The pulp's $t_{½}$ is over an order of magnitude greater than CNCs, at this temperature. This clearly illustrates the impact of hydrolysis and the residual sulfate esters on the surface of the CNCs. However, these results indicate that the CNCs should be stable in the composites during typical cure and application conditions. The effect of oxygen has not yet been ascertained; however, the epoxy resin can be expected to protect the CNCs for oxygen under normal use.

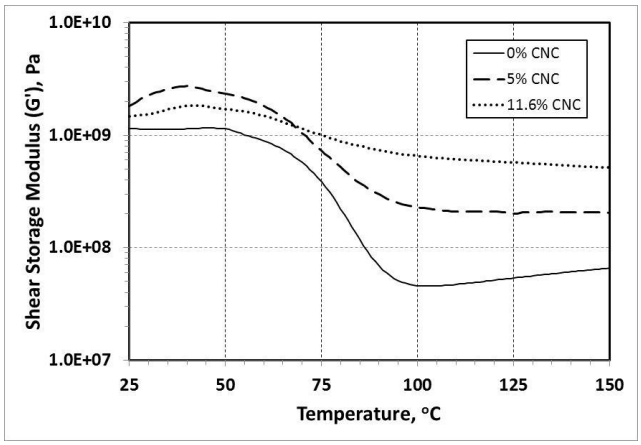

Figure 4: G' versus temperature data from DMTA thermoscans of epoxy (0% CNC) and epoxy with 5 and 11.6 wt.% CNCs [10].

The change in stiffness of the epoxy and CNC composites as a function of temperature from 25 to 150°C is shown in Figure 4. At temperatures below T_g the moduli of the CNC composites is overall higher than then neat epoxy. This increase is unusually inconsistent with CNC loading levels. This becomes consistent with loading near the T_g. At temperatures above T_g the moduli of the CNC composites are significantly increased over that of the neat epoxy. This indicates a marked shift in the effective cross-linked network to a system of more densely populated interactions. The 11.6 wt.% composite exhibits very little change in modulus above T_g. Such properties are generally indicative of enhanced strength at elevated temperatures something that is advantageous in industrial applications for extended use temperatures and/or load carry capacity at $T>T_g$.

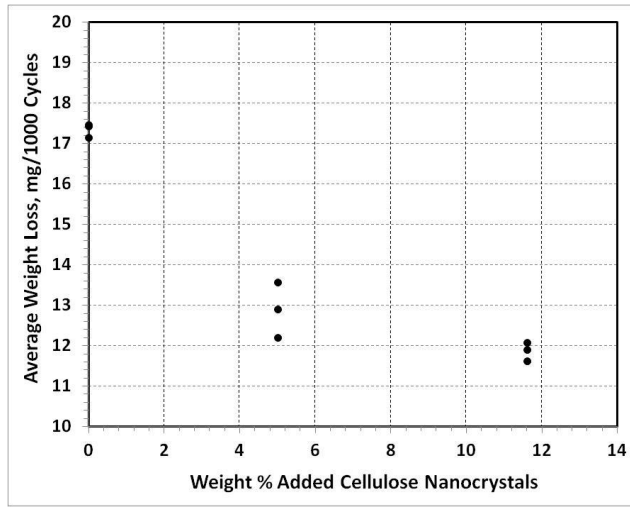

Figure 5: Average weight loss per 1000 cycles of Taber abrasion versus added wt.% CNCs [10].

The industrial grade WB epoxy formulation adapted for this research is targeted at metal protection applications. Thus, the abrasion resistance of the composite coatings was ascertained via a Taber abrader. Figure 5 shows the results of this testing where the average weight loss per 1000 cycles is plotted versus the wt.% added CNCs. The results of the Taber method is strongly affected by contamination of the abrading wheels with particles removed from the coating. Increasing or decreasing the period between cleaning with sand paper will have a similar effect on abrasion resistance results. Addition of 5 wt.% CNCs significantly reduced the weight loss. This is further decreased by addition of 11.6 wt.% CNCs although it appears to be reaching a plateau. This result is surprising from the standpoint of addition of a biobased material to an epoxy for increased abrasion. The result is supported by the DMA results indicating significant levels of reinforcement imparted by the CNCs.

Conclusions

An industrial grade WB epoxy coating formulation was adapted for use with CNC aqueous dispersions. The resultant CNC composites have very good dispersion as qualitatively evidenced by the absence of phase separated domains under cross polarized optical microscopy. The addition of CNCs resulted in a decreased thermal stability at temperatures above 150°C most likely due to loss of moisture hydrogen bonded to the CNCs. Thermal stability of the CNCs and source pulp was investigated via the Kissinger method. This showed that the CNCs have substantially reduced thermal stability compared to the source pulp, likely due to the residual sulfuric acid esters imparted during hydrolysis.

Thermal mechanical testing revealed a significant increase in modulus below T_g that is substantially greater above T_g, in the rubber plateau region. The latter result is taken in the CNC research field as evidence of percolation

between the CNC fibers such that a denser network of interconnected components exist within the composite [7]. The 11.6 wt.% composite showed only a slight drop in modulus above T_g where the epoxy decreased by more than an order of magnitude in the same temperature regime. Taber abrasion testing demonstrated that the CNCs can significantly reduce the weight loss of the coating. Thus the composite films are expected to provide protection to the under lying substrate for longer periods of service life.

Acknowledgements

The authors would like to gratefully acknowledge partial support of this work by U.S. Forest Service Grant 10-JV-11111104-066 and Richard Reiner/Alan Rudie of the Forest Products Laboratory for providing the CNCs used in this study. We are also grateful to Air Products for providing the epoxy, curing agent, and defoamers.

References

[1] R.O. Herzog, W. Jancke, Über den Physikalischen Aufbau einiger Hochmolekularer Organisher Verbindungen, Ber Dtsch Chem Ges, 53 (1920) 2162-2164.
[2] P. Scherrer, Bestimmung der Inneren Struktur and der Grösse von Kolloidteilchen mittels Röntgenstrahlen, in: R. Zsigmondy (Ed.) Kolloidchemie: ein Lehrbuch, Spamer, Leipzig, 1920.
[3] B.G. Ranby, Aqueous Colloidal Solutions of Cellulose Micelles, Acta Chemica Scandinavica, 3 (1949) 649-650.
[4] B.G. Ranby, E. Ribi, Über den Feinbau der Zellulose, Experientia, 6 (1950) 12-14.
[5] B.G. Ranby, Cellulose and Muscle - The Colloidal Properties of Cellulose Micelles, Discussions of the Faraday Society, (1951) 158.
[6] B.G. Ranby, The Cellulose Micelles, Tappi, 35 (1952) 53-58.
[7] R.J. Moon, A. Martini, J. Nairn, J. Simonsen, J. Youngblood, Cellulose Nanomaterials Review: Structure, Properties and Nanocomposites, Chemical Society Reviews, 40 (2011) 3941-3994.
[8] R.S. Reiner, A.W. Rudie, *Process Scale-Up of Cellulose Nanocrystal Production to 25 kg per Batch at the Forest Products Laboratory*, in: M.T. Postek, R.J. Moon, A.W. Rudie, M.A. Bilodeau (Eds.) Production and Applications of Cellulose Nanomaterials, Tappi Press, Peachtree Corners, GA, 2013, pp. 22-24.
[9] A. International, ASTM D4060-10 Standard Test Method for Abrasion Resistance of Organic Coatings by the Taber Abraser, Annual Book of ASTM Standards, ASTM International, West Conshohocken, PA, 2010, pp. 505-509.
[10] L. Cross, G. Schueneman, E. Mintz, Polymer Matrix Nanocomposites via Forest Derived Nanomaterials, Proceedings of NSTI Nanotechnology 2012 ConferenceSanta Clara, CA, 2012.
[11] H.E. Kissinger, Reaction Kinetics in Differential Thermal Analysis, Analytical Chemistry, 29 (1957) 1702-1706.
[12] A.P. Snyder, W.M. Maswadeh, C.H. Wick, J.P. Dworzanski, A. Tripathi, Comparison of the kinetics of thermal decomposition of biological substances between thermogravimetry and a fielded pyrolysis bioaerosol detector, Thermochimica Acta, 437 (2005) 87-99.